JMEPEG (2010) 19:1172–1182
DOI: 10.1007/s11665-010-9613-5

1059-9495/$19.00

A Study of the Tensile Deformation and Fracture Behavior of Commercially Pure Titanium and Titanium Alloy: Influence of Orientation and Microstructure

U. Bathini, T.S. Srivatsan, A. Patnaik, and T. Quick

(Submitted September 22, 2009; in revised form December 21, 2009)

In this paper, the tensile deformation and fracture behavior of commercially pure titanium and the titanium alloy (Ti-6Al-4V) are presented and briefly discussed. Samples of both commercially pure titanium and the Ti-6Al-4V alloy were prepared from the as-provided plate stock along both the longitudinal and transverse orientations. The specimens were then deformed to failure in uniaxial tension. The intrinsic influence of material composition and test specimen orientation on microstructure, tensile properties, and resultant fracture behavior of the two materials is presented. The conjoint influence of intrinsic microstructural features, nature of loading, and specimen orientation on tensile properties of commercially pure titanium and the Ti-6Al-4V alloy is highlighted. The fracture behavior of the two materials is discussed taking into consideration the nature of loading, specimen orientation, and the role and contribution of intrinsic microstructural effects.

Keywords commercially pure titanium, microstructure, tensile fracture, tensile properties, titanium alloy

1. Introduction

In the continuing era of rapid industrial revolution and resultant growth, noticeable advances in the domains of basic sciences, engineering and related technologies have gradually focused on the development, emergence, and extended use of the traditional metals, their alloy counterparts, and in more recent years their composite counterparts, i.e., composites based on metal matrices also referred to as metal-matrix composites (MMCs). One such metal is titanium, which has grown in stature, strength, and preferential use arising from need during the last three decades, i.e., since the early 1970s (Ref 1, 2). Due to a combination of excellent mechanical properties spanning specific strength (σ_{UTS}/ρ), stiffness, corrosion and erosion resistance, fracture toughness, formability and capability to withstand both high temperatures and low temperatures, sustained research efforts have led to the development, emergence, and use of titanium alloys for a range of performance—critical and high-performance-related applications (Ref 3, 4).

Over the years the aerospace industry has evolved from a purely defense-driven environment that pushed technology to its limits to one largely controlled by commercial interests. Today, issues like off-the-shelf availability, long-term cost effectiveness, smart material options, and high life cycle design are the primary consideration in the selection criteria. Adding these issues to the development conditions has not kept the material scientists from responding with new and innovative ideas. While this environment may limit the discovery of new materials, scientists and engineers continue to make refinements and develop new alloys and processes. Besides the aluminum alloys, titanium and its alloys find selection and use as a metal for a variety of aerospace applications (Ref 5).

Pure titanium metal has a melting point of 1675 °C and an atomic weight of 47.9 (Ref 6). The density of pure titanium metal is 4.5 g/cm^3, which is about 60% of steel (Ref 2, 6). Furthermore, pure titanium metal and its alloy counterparts are essentially non-magnetic and offer good heat transfer capability. The excellent specific strength [σ_{UTS}/ρ] of pure titanium and its alloys at both high temperature (in excess of 590 °C) and low temperature (less than −253 °C) enables it to be the preferred metal that is often chosen and used as an ultra high speed metal for aircraft structural components and even components of the space shuttle (Ref 3, 4, 6). The high melting point of titanium metal enables it to be considered for use in turbine engines (Ref 7). With their high strength performance at elevated temperatures, titanium alloys were the primary structural material (about 95 pct) used in the SR-71 Blackbird more than 30 years ago. To this day, the Blackbird remains the premier high-speed research aircraft. Titanium alloys have improved their high-temperature capabilities from about 400 °C 30 years ago to more than 600 °C today. This improvement has been followed by the increased selection and use of titanium alloys in both the military and commercial aircraft. In 1966, about 1% of the weight of a Boeing 707 was titanium, compared to 10% in today's 747. As recently as 2005, the Boeing Aerospace Company used 15 million pounds of the titanium metal, i.e., various alloys, in different versions of their commercial aircraft. This usage was expected to more than

U. Bathini and **A. Patnaik**, Department of Civil Engineering, The University of Akron, Akron, OH 44325; **T.S. Srivatsan**, Department of Mechanical Engineering, The University of Akron, Akron, OH 44325; and **T. Quick**, Department of Geology, The University of Akron, Akron, OH 44325. Contact e-mail: tsrivatsan@uakron.edu.

double when production of the 787 dreamliner commenced, which in essence was planned to have 20% of the primary structure to be the titanium metal (Ref 8). Apart from the BOEING Company, other manufacturers of both commercial aircraft and military aircraft will enhance their use of the titanium metal for a spectrum of high-performance-related products. Furthermore, since the titanium metal has excellent super plastic properties, it can be easily deformed to the tune of 2000% without experiencing appreciable necking and/or cracking when heated to a temperature of 925 °C during the super-plastic forming process. Also, titanium and its alloy counterparts are nonmagnetic and have a lower linear coefficient of expansion and lower thermal conductivity than the widely chosen and used family of steel and the alloys of aluminum (Ref 9). In more recent years, the automotive industry has increased its use of the titanium alloys because of its performance at elevated temperatures coupled with good formability. Noticeably, the metal has minimal degradation and high oxidation resistance during prolonged long-term service or extended service at elevated temperatures (Ref 3, 4). In the health industry, titanium has grown in strength to find use as implants since it is biocompatible. Overall, while procurement of the raw material, manufacturing, production and processing, to include both primary and secondary, of titanium alloys may be expensive, its overall combination of attractive physical and mechanical properties offsets its high cost (Ref 2, 10).

Most noticeably, titanium is allotropic and has a hexagonal close packed (HCP) {α} crystal structure at low temperatures and a body-centered cubic (β) structure at temperatures above 885 °C (Ref 4, 6). The family of titanium alloys is essentially categorized as being corrosion resistant or structural. The structural titanium alloys are classified into three categories, denoted as α, α + β, and the β phase alloys. The alpha-phase alloys of titanium, which are categorized as commercially pure titanium, are relatively weak in strength but offer a combination of good corrosion resistance, good weldability, acceptable creep resistance, receptive to heat treatment coupled with ease of processing and fabrication (Ref 1, 2). The beta-phase alloys are receptive to forging while concurrently offering excellent fracture toughness. The dual phase [i.e., alpha + beta] alloys offer a combination of excellent ductility and strength when properly heat treated, which makes them stronger than both the alpha-phase and beta-phase counterparts (Ref 4, 6, 8, 11).

The objective of the present investigation was to establish the influence of test specimen orientation and material microstructure on tensile deformation and fracture behavior of commercially pure titanium metal (Grade 2) and the alloy Ti-6Al-4V. The study presented in this article is part of a larger ongoing research program aimed at establishing the influence of orientation of plate and microstructure on the structural response of welded titanium structures. A research endeavor of interest, of significance to and needed for the US Army based in Picatinny Arsenal for the use of titanium for several battle-related applications. The titanium material, i.e., the commercially pure (Grade 2) and the alloy (Ti-6Al-4V) were provided as plate stock in the annealed condition. Test specimens machined from the two materials were carefully deformed in uniaxial tension on a fully automated mechanical test machine at ambient temperature (27 °C) and relative humidity of 55 pct. The tensile properties and final fracture behavior of the commercially pure (CP) titanium (Grade 2) and the Ti-6Al-4V alloy are discussed in light of test specimen orientation (longitudinal versus transverse), nature of loading (uniaxial tension), local stress state, intrinsic microstructural features and deformation characteristics of the microstructure.

2. Materials

The materials chosen for this research study are the commercially pure titanium (Grade 2), referred to henceforth through this article as CP (Grade 2), and the widely preferred and chosen alloy, also referred to as the 'workhorse' alloy, Ti-6Al-4V. The CP (Grade 2) titanium material was provided by TICO (based in Michigan) while the Ti-6Al-4V alloy was provided by Allegheny Technologies ATI Wah Chang (based in Oregon). The advantage favoring the selection and use of the Ti-6Al-4V alloy is that it is comparatively easy to produce coupled with good hot workability and receptive to heat treatment, thereby enabling a lenient window of processing parameters (Ref 12-17). Both the CP (Grade 2) and the Ti-6Al-4V alloy are receptive to heat treatment and can be solution heat treated and annealed to achieve the desired strength and properties. The two materials, CP titanium (Grade 2) and Ti-6Al-4V, were provided by the manufacturers in the fully annealed condition. The nominal composition of the two chosen materials is provided in Table 1.

3. Experimental Procedures

3.1 Sample Preparation

The tensile tests were conducted on test specimens that were precision machined from both the longitudinal (L) and transverse (T) orientation of the as-provided annealed plate stock. The longitudinal (L) specimens were machined with the major stress axis parallel to the rolling direction of the CP (Grade 2) and Ti-6Al-4V titanium alloy plates, while the transverse (T) specimens were machined with the major stress axis perpendicular to the rolling direction of CP (Grade 2) and Ti-6Al-4V alloy plates. The cylindrical test specimens conformed well with the specifications outlined in the standard ASTM E-8 and had threaded ends. At the gage section, the test specimens measured 3.125 mm in diameter and 12.5 mm in length. A schematic of the test specimen is shown in Fig. 1. To minimize the effects and/or contributions from surface irregularities and finish, final surface preparation was achieved by mechanically polishing the gage section of the machined test specimens with progressively finer grades of silicon carbide impregnated emery paper (320 grit, 400 grit, and 600 grit) to remove all circumferential scratches and any residual machine marks.

Table 1 Nominal chemical composition of the two chosen titanium materials (in wt.%)

Material	Ti	Al	N	V	C	Fe	H	O
Ti-6Al-4V	90.0	6.0	0.05	4.0	0.1	0.4	0.02	0.20
CP (Grade 2)	99.35	…	0.03	…	0.1	0.3	0.01	0.20

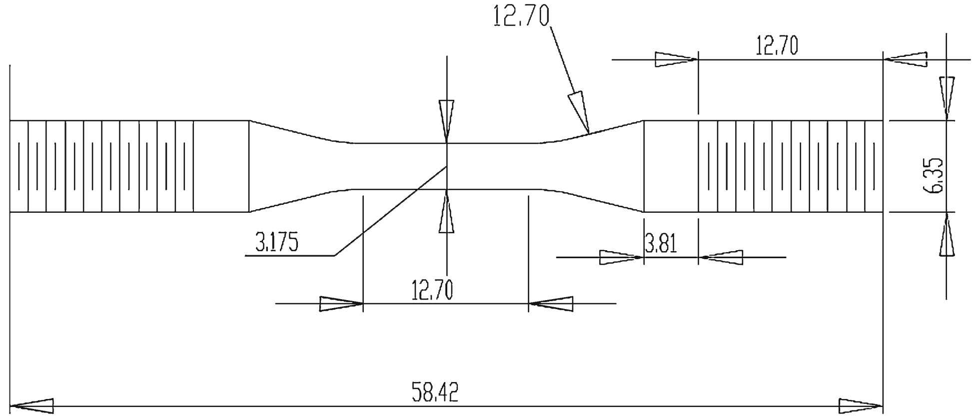

ALL DIMENSIONS ARE IN MILLIMETERS

Length of the threaded section	= 12.70 mm
Length of the shoulder	= 3.81 mm
Diameter of the grip section	= 6.35 mm
Diameter of the reduced section	= 3.175 mm
Gage length	= 12.70 mm
Overall length	= 58.42 mm
Fillet radius	= 12.70 mm

Use 6.35 mm diameter x 20 TPI threads

Fig. 1 A schematic of the longitudinal and transverse flat test specimen used for mechanical testing (tensile and cyclic fatigue)

3.2 Initial Microstructure Characterization

An initial characterization of the microstructure of the as-provided material was done using a low magnification optical microscope. Samples of desired size were cut from the as-received stock of the commercially pure (Grade 2) and Ti-6Al-4V titanium alloy and mounted in bakelite. The mounted samples were then wet ground on progressively finer grades of silicon carbide impregnated emery paper using copious amounts of water both as a lubricant and as a coolant. Subsequently, the ground samples were mechanically polished using 5-μm diamond solution. Fine polishing to a perfect mirror-like finish of the surface of each titanium material, i.e., CP (Grade 2) and Ti-6Al-4V alloy, was achieved using 1-μm diamond solution as the lubricant. The polished samples were subsequently etched using a reagent that is a solution mixture of 5-mL of nitric acid (HNO_3), 10 mL of hydrofluoric acid (HF), and 85 mL of water (H_2O). The polished and etched surface of the samples of CP (Grade 2) and Ti-6Al-4V alloy was observed in an optical microscope and photographed using bright field illumination technique.

3.3 Mechanical Testing

Uniaxial tensile tests on the longitudinal and transverse specimens of both CP Ti (Grade 2) and the Ti-6Al-4V alloy were performed on a fully automated, closed-loop servo-hydraulic mechanical test machine [INSTRON-8500 Plus] using a 100 kN load cell. The tensile tests were conducted at room temperature (300 K) and in the laboratory air (relative humidity of 55 pct) environment. The test specimens were deformed to failure at a constant strain rate of 0.0001/s. An axial 12.5-mm gage length clip-on type extensometer was attached to the test specimen at the gage section using rubber bands. The stress and strain measurements, parallel to the load line, and the resultant mechanical properties, such as stiffness, strength (yield strength and ultimate tensile strength), failure stress and ductility (strain-to-failure), were provided as a computer output by the control unit of the mechanical test machine.

3.4 Failure-Damage Analysis

The fracture surfaces of the deformed and failed tensile specimens of CP Ti (Grade 2) and Ti-6Al-4V alloy were comprehensively examined in a scanning electron microscope (SEM) to determine the macroscopic fracture mode and to concurrently characterize the fine scale topography and intrinsic features on the tensile fracture surface for the purpose of establishing the microscopic mechanisms governing fracture. The distinction between the macroscopic fracture mode and microscopic fracture mechanisms is based entirely on the magnification level at which the observations are made. The macroscopic mode essentially refers to the overall nature of failure while the microscopic mechanisms relate to the local failure processes, such as (i) microscopic void formation, (ii) microscopic void growth and coalescence, and (iii) nature, intensity, and severity of the fine microscopic cracks and macroscopic cracks dispersed through the fracture surface. The samples for observation in the scanning electron microscope (SEM) were obtained from the failed tensile specimens of both CP Ti (Grade 2) and the Ti-6Al-4V alloy by sectioning parallel to the fracture surface.

4. Results and Discussion

4.1 Initial Microstructure

The microstructure of an alloy is an important factor that determines its mechanical properties to include tensile properties, fracture toughness, fatigue resistance, and resultant fracture behavior. The optical microstructure of the CP Ti (Grade 2) is shown in Fig. 2 and the Ti-6Al-4V alloy is shown in Fig. 3 at three different magnifications. These two figures essentially reveal the as-received, undeformed microstructure of the two chosen materials to be noticeably different. The observable difference is primarily in the volume fraction, morphology, size, and distribution of the intrinsic micro-constituents through the microstructure:

(i) Low magnification observation of the microstructure of the high-purity CP (Grade 2) titanium essentially revealed the primary alpha (α) grains to be intermingled with small yet noticeable pockets of the beta (β) grains. High-magnification observation revealed very fine alpha (α) phase lamellae located within the beta (β) grain (Fig. 2b).

(ii) Observations of the Ti-6Al-4V alloy over a range of magnifications spanning very low to high magnification revealed a duplex microstructure consisting of the near equiaxed alpha (α) and transformed beta (β) phases. The primary near equiaxed shaped alpha (α) grains (light in color) were well distributed in a lamellar matrix having transformed beta (dark in color) (Fig. 3). The size of both the alpha grains and the transformed β grains range from 5 to 15 μm. The presence of trace amounts of aluminum and oxygen in the Ti-6Al-4V alloy contributes to stabilizing and strengthening the alpha (α) phase, which is overall beneficial for enhancing hardenability, increasing strength, and improving the response kinetics of the alloy to heat treatment (Ref 18).

At equivalent high magnification (500×), the observable differences in intrinsic microstructural constituents of the two titanium materials, i.e. CP Ti (Grade 2) and the Ti-6Al-4V, are shown in Fig. 2(c) and 3(c) bringing out clearly the size, morphology, volume fraction, and distribution of the alpha (α) and beta (β) phases.

4.2 Tensile Response

The room temperature tensile properties of CP Ti (Grade 2) and the Ti-6Al-4V alloy are summarized in Table 2. The results reported are the mean values based on duplicate tests. The elastic modulus, yield strength, ultimate tensile strength, elongation to failure and strength at failure (fracture) were

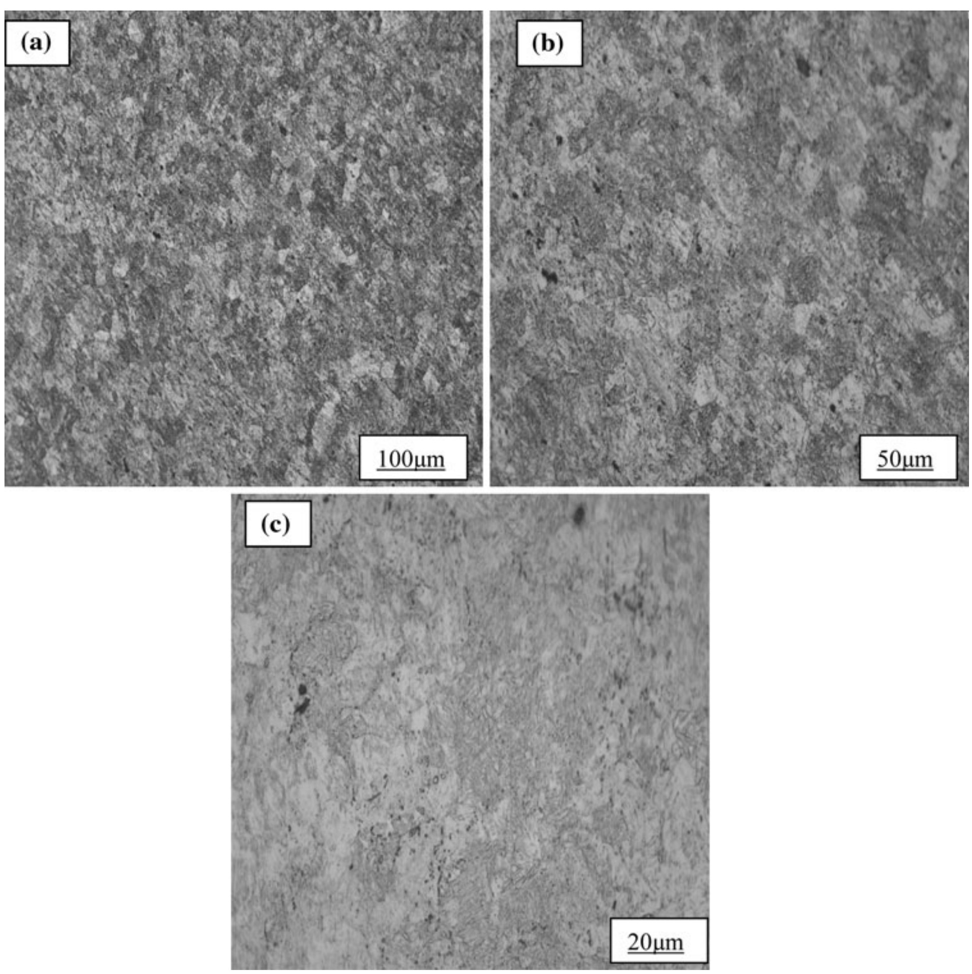

Fig. 2 Optical micrographs showing the key micro-constituents in the commercially pure (Grade 2) titanium at three different magnifications

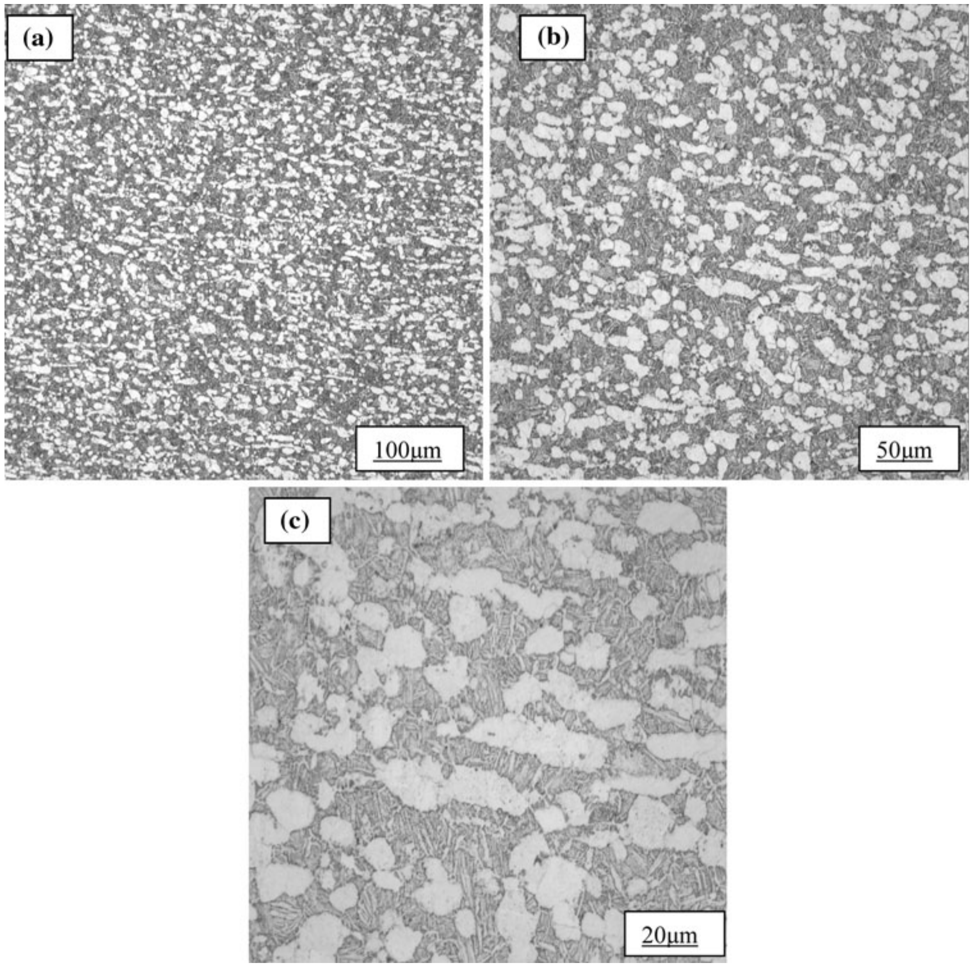

Fig. 3 Optical micrographs showing the key micro-constituents, their morphology and distribution, in the Ti-6Al-4V alloy at three different magnifications

Table 2 Room temperature tensile properties of Ti- 6Al-4V and commercially pure (Grade 2) (results are mean values based on duplicate tests)

		Elastic modulus, E(a)		Yield strength, σ_{YS}		UTS, σ_{UTS}				
Material	**Orientation**	**msi**	**GPa**	**ksi**	**MPa**	**ksi**	**MPa**	**Elongation GL = 0.5″, %**	**Reduction in area, %**	**Tensile ductility $\ln(A_o/A_f)$, %**
Commercially pure	Longitudinal (L)	16	115	63	432	81	561	14.7	43.4	57
Ti (Grade 2)	Transverse (T)	15	108	55	382	67	465	18.9	47	63
Ti-6Al-4V	Longitudinal (L)	18	126	134	921	148	1020	7.8	23.8	27
	Transverse (T)	20	137	149	1029	167	1153	11.5	21.7	25

(a) The values of young's modulus have been calculated from the linear portion of the curve representing the engineering stress-engineering strain relationship

provided as an output of the PC-based data acquisition system. The elastic modulus (E) was also determined from the slope of the linear portion of the engineering stress versus engineering strain curve. The yield strength was determined by identifying the stress at a point on the engineering stress versus engineering strain curve where a straight line drawn parallel to the elastic portion of the stress versus strain curve at 0.2% offset intersects the curve. The ductility is reported as elongation-to-failure over a gage length of 12.7 mm. This elongation of the test specimen was measured using a clip-on extensometer that was attached to the gage section of the test specimen.

4.2.1 Commercially Pure (Grade 2). The elastic modulus of this material as determined from slope of the linear region if the engineering stress versus engineering strain curve is 115 GPa in the longitudinal orientation and 108 GPa in the transverse orientation. For this CP titanium (Grade 2), the yield strength is 432 MPa (63 ksi) in the longitudinal orientation and 15 pct higher than in the transverse orientation [382 MPa (55 ksi)].

The ultimate tensile strength is 561 MPa (81 ksi) in the longitudinal orientation and 465 MPa (67 ksi) in the transverse orientation, a noticeable difference of 20 pct. The ultimate tensile strength is higher than the yield strength, indicating a noticeable work hardening beyond yield. The elongation of CP (Grade 2) was 14.7% in the longitudinal orientation and 18.9% in the transverse orientation. The reduction-in-area was 43.4% in the longitudinal orientation and 47% in the transverse orientation. The engineering stress versus engineering strain curves for the material in both the longitudinal and transverse orientations are shown in Fig. 4.

The stress versus strain curve for this metal in the region of plastic deformation can be expressed by the power law relation:

$$\sigma = K\varepsilon^n \qquad \text{(Eq 1)}$$

where n is the strain hardening exponent and K is the strength coefficient. A plot of the true stress versus true strain data, up to the maximum load, on a logarithmic scale will result in a straight line if the above equation is satisfied by the test data. The linear slope of this line is n and K is the true stress at $\varepsilon = 1$. Variation of true stress with true strain, as shown in Fig. 5, reveals the CP titanium (Grade 2) to be

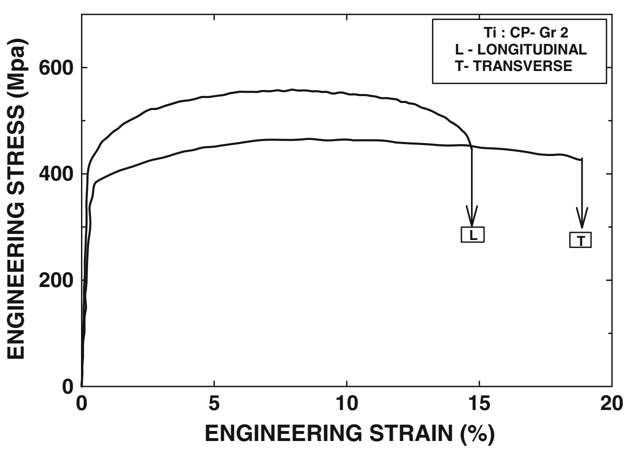

Fig. 4 Influence of test specimen orientation on engineering stress vs. engineering strain curve for commercially pure (Grade 2) titanium

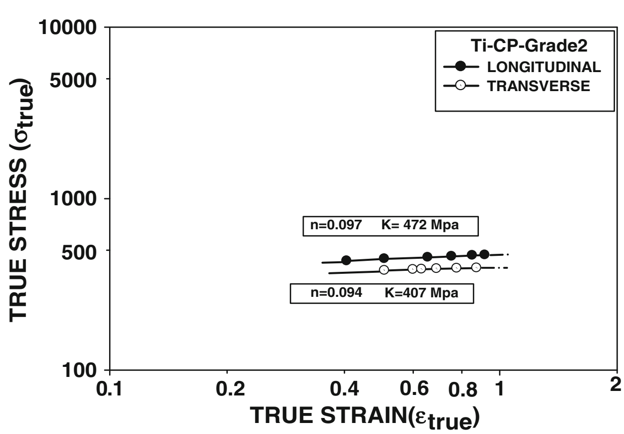

Fig. 5 The monotonic stress vs. strain curve for the commercially pure (Grade 2) titanium

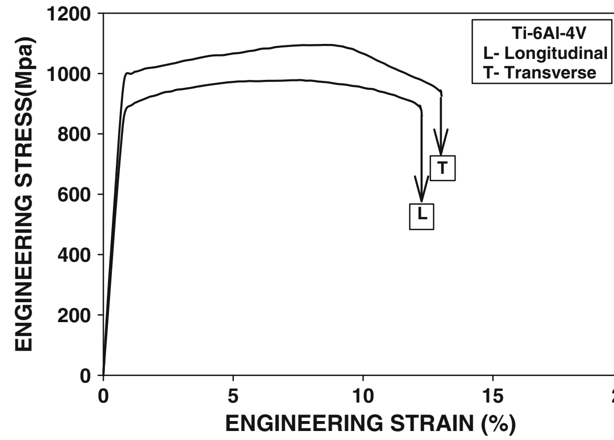

Fig. 6 Influence of test specimen orientation on engineering stress vs. engineering strain curve of Ti-6Al-4V alloy

harder in the longitudinal orientation when compared to the transverse orientation. The strain hardening exponent (n) of this material is 0.097 in the longitudinal orientation and 0.094 in the transverse orientation.

4.2.2 Ti-6Al-4V Alloy. A representative engineering stress versus engineering strain curve for the two orientations of the as-received plate, i.e., longitudinal and transverse, is shown in Fig. 6. The elastic modulus of the alloy is 126 GPa in the longitudinal orientation and 137 GPa in the transverse orientation and is a measure of the slope of the linear region of the stress versus strain curve. The yield strength of the alloy in the annealed condition is 948 MPa (137 ksi) in the longitudinal orientation and 1047 MPa (152 ksi) in the transverse orientation. The ultimate tensile strength of the alloy is 1060 MPa (154 ksi) in the longitudinal orientation and 1181 MPa (171 ksi) in the transverse orientation. The ultimate tensile strength of the Ti-6Al-4V alloy is marginally higher than the yield strength, i.e., about 10%, indicating the work hardening rate beyond yield to be low. The elongation-to-failure (ε_f) of the alloy is 7.8% in the longitudinal orientation and 11.5% in the transverse orientation. The reduction-in-area of the alloy was 24% in the longitudinal orientation and 22% in the transverse orientation and accords well with the annealed condition of the alloy microstructure. The yield strength and tensile strength values of the alloy conform well to the values obtained and reported by the manufacturer (ATI Wah Chang) and recorded in ASM Metals Handbook (Ref 1). Variation of true stress with true strain, as shown in Fig. 7, reveals the Ti-6Al-4V to be marginally harder in the transverse orientation when compared to the longitudinal orientation. The slope of the true stress versus true strain line is the strain hardening exponent (n) of the alloy and it is 0.095 in the transverse orientation and 0.085 in the longitudinal orientation.

4.3 Tensile Fracture Behavior

An exhaustive examination of the tensile fracture surfaces of both the longitudinal and transverse specimens in a scanning electron microscope (SEM) revealed the specific role played by intrinsic microstructural features and microstructural effects on strength and ductility properties of the chosen titanium material. Representative fractographs of the tensile fracture surface of CP (Grade 2), for the longitudinal specimen, are shown in Fig. 8 and the transverse specimen in Fig. 9. For the

Ti-6Al-4V alloy, the intrinsic fracture features for the longitudinal specimen are shown in Fig. 10 and for the transverse specimen in Fig. 11.

4.3.1 The Ti-6Al-4V Alloy. At the macroscopic level, tensile fracture of the test specimen machined from longitudinal orientation of the plate stock was essentially normal to the far-field stress axis. Overall morphology of the tensile fracture surface appeared to be rough and layered (Fig. 10a). Observation of the fracture surface at higher magnifications revealed a combination of macroscopic (Fig. 10b) and fine microscopic cracks coupled with a healthy population of shallow dimples, of varying size and shape, covering the transgranular fracture surface (Fig. 10c). At the higher allowable magnification of the SEM, a population of fine microscopic voids and shallow dimples were found covering the region of tensile overload (Fig. 10d). An observation of the fracture surface of the same test specimen same fracture surface at a different location revealed the transgranular regions to be covered with pockets of shallow dimples and randomly distributed fine microscopic voids. The morphology of the fine microscopic voids on the transgranular fracture surface can be seen in Fig. 10(d).

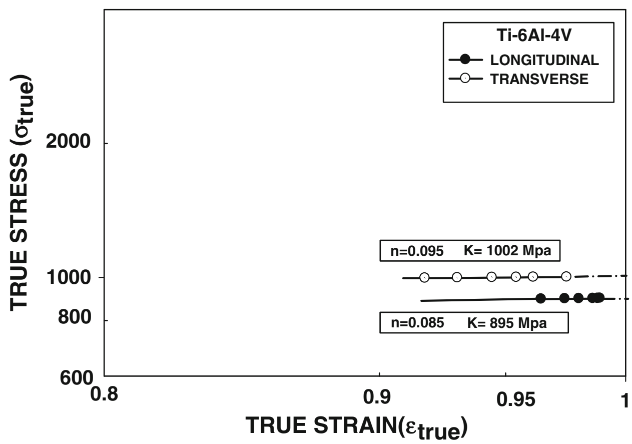

Fig. 7 The monotonic stress vs. strain curve for the Ti-6Al-4V alloy

The fractographs of the test specimen machined from the transverse orientation of the as-provided plate stock are shown in Fig. 11. The failure was typical cup and cone type. The overall morphology of the cone surface was rough (Fig. 11a). An array of macroscopic and microscopic cracks were surrounded by a population of dimples and voids of varying size, features reminiscent of both locally brittle and locally ductile failure mechanisms (Fig. 11b). At regular intervals, deep-seated microscopic cracks were evident on the fracture surface (Fig. 11c). The microscopic cracks result as a consequence of the growth and eventual coalescence of the fine microscopic voids. The overload

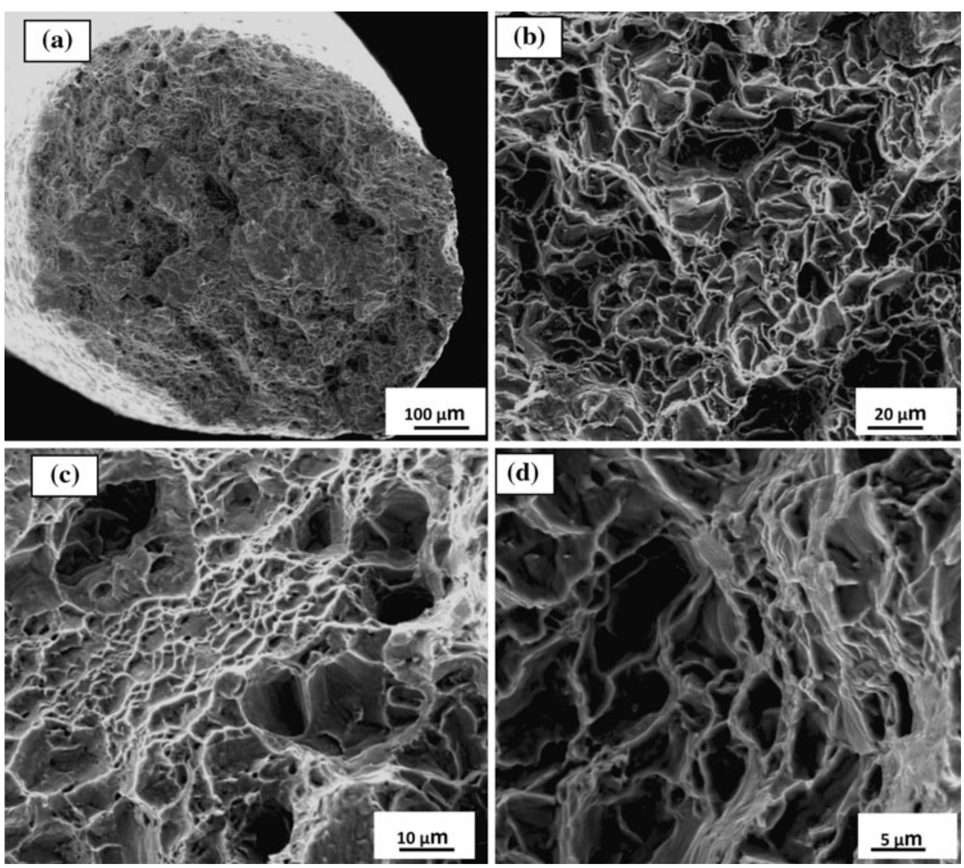

Fig. 8 Scanning electron micrographs of the tensile fracture surface of commercially pure titanium (Grade 2) specimen (orientation: longitudinal) deformed in tension, showing (a) overall morphology of tensile fracture surface at an inclination to stress axis; (b) high magnification of (a) showing population of voids and shallow dimples of varying size covering the transgranular region; (c) high magnification of (b) showing the morphology and distribution of dimples and fine microscopic cracks features reminiscent of locally ductile and brittle failure mechanisms; (d) the overload region showing microscopic voids, cracks and shallow dimples

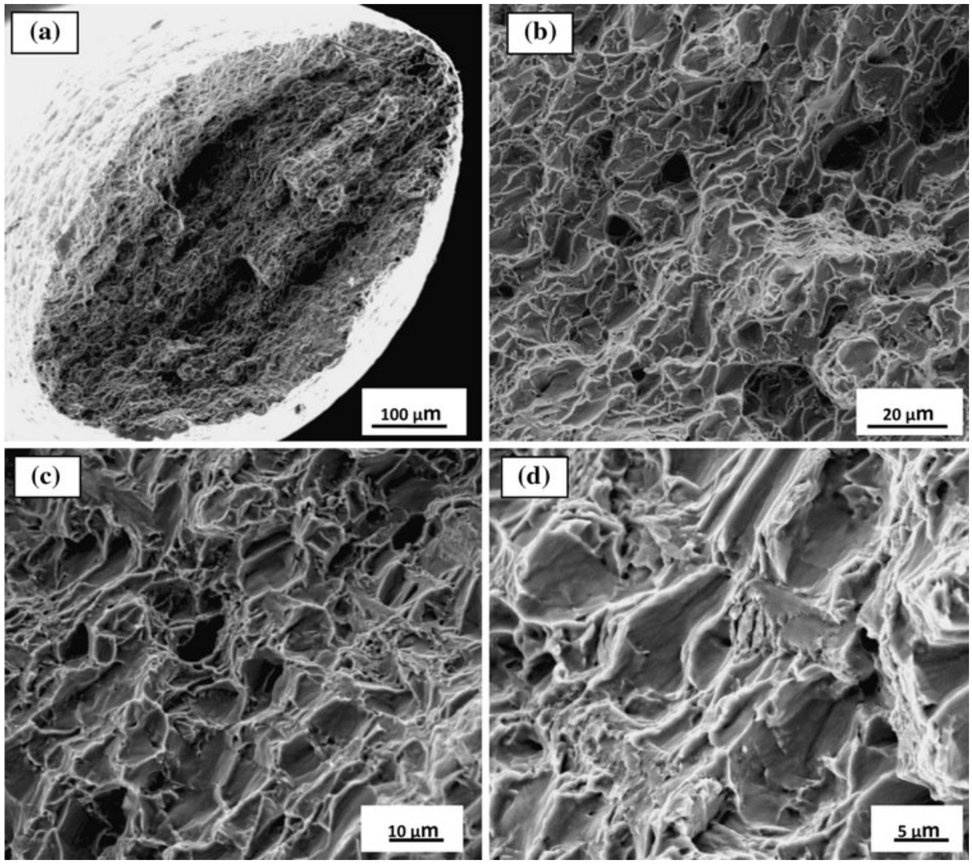

Fig. 9 Scanning electron micrographs of the tensile fracture surface of commercially pure titanium (Grade 2) specimen (orientation: transverse) deformed in tension, showing (a) overall morphology of tensile fracture surface at an inclination to stress axis; (b) high magnification of (a) showing isolated voids and shallow dimples of varying size covering the transgranular region; (c) high magnification of (b) showing the morphology and distribution of dimples and fine microscopic voids features reminiscent of locally ductile failure mechanisms; (d) the overload region showing randomly distributed microscopic voids, microscopic cracks and pockets of shallow dimples

region revealed a population of dimples of varying size and shape, and fine microscopic voids (Fig. 11d), features reminiscent of locally ductile failure mechanisms. Overall, the presence of a sizeable population of fine microscopic voids and macroscopic voids coupled with isolated microscopic cracks contributes to lowering of the actual strain-to-failure associated with ductile fracture. Isolated cracks in deep pockets, surrounded by a population of shallow dimples of varying size and fine microscopic voids, were observed at higher magnification (Fig. 11b). A detailed observation of the transgranular surface region at higher magnifications revealed the fine microscopic cracks to be surrounded by a population of microscopic voids and dimples reminiscent of locally brittle and ductile failure mechanisms. The dimples observed were of varying size but shallow in depth. While the macroscopic failure mode was different, the microscopic fracture surface features were identical in the two orientations, longitudinal and transverse, of the alloy plate.

4.3.2 CP (Grade 2). On a macroscopic scale, tensile fracture of this material in the longitudinal orientation was at an inclination to the far-field stress axis (Fig. 8a). Careful observation of the different regions of the fracture surface was made at high magnification to delineate the intrinsic fracture features. Isolated and randomly distributed microscopic voids and a healthy population of ductile dimples were found covering the transgranular fracture regions (Fig. 8b). High-magnification observations in the transgranular region revealed the dimples to be shallow and of varying size coupled with fine microscopic cracks (Fig. 8c). The overload region revealed a healthy combination of fine microscopic cracks, microscopic voids of varying size and randomly distributed through the surface, and a large population of shallow dimples, features reminiscent of locally brittle and ductile failure mechanisms (Fig. 8d).

For the test specimen machined from the transverse orientation of the plate, overall morphology of the tensile fracture surface was at an inclination to the tensile stress axis (Fig. 9a). High-magnification observation in the transgranular region revealed features that were quite similar to the longitudinal counterpart, i.e., a combination of microscopic voids of varying size and a large population of ductile dimples (Fig. 9b). The dimples were shallow in nature and of varying size (Fig. 9c). Observation in the tensile overload region revealed features that were quite similar to those observed in the transgranular region, i.e., microscopic voids of varying size and shallow dimples of non-uniform size and shape. The features observed through the fracture surface were reminiscent of locally ductile and brittle failure mechanisms governing the tensile response of CP (Grade 2) titanium. Essentially, the macroscopic fracture mode and microscopic fracture features were identical in the two orientations, longitudinal and transverse, of the alloy plate.

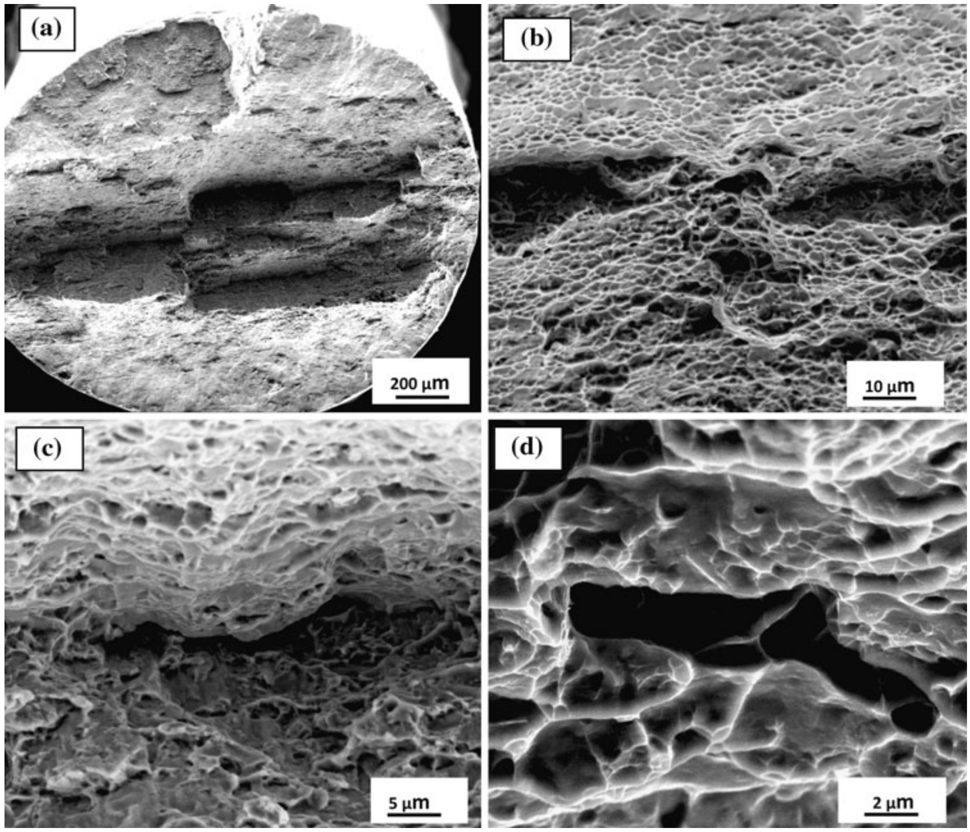

Fig. 10 Scanning electron micrographs of the tensile fracture surface of Ti-6Al-4V specimen (orientation: longitudinal) deformed in tension, showing (a) overall morphology of tensile fracture surface; (b) high magnification of (a) showing macroscopic crack in the transgranular region; (c) a microscopic crack surrounded by population of shallow dimples; (d) the overload region showing coalescence of microscopic voids to form a microscopic crack and surrounded by shallow dimples

4.4 Mechanisms Governing Tensile Deformation and Fracture

Due to the occurrence and presence of fairly high localized stress intensities at selected points through the microstructure, the corresponding strain is conducive for:

(i) the nucleation and early growth of the microscopic voids, and
(ii) the eventual coalescence of the microscopic and macroscopic voids to occur at low to moderate stress levels (Ref 18, 19).

This results in the early initiation and presence of fine microscopic cracks distributed through the fracture surface (Ref 20). During far-field loading, the fine microscopic voids tend to grow, or increase in size, and eventually impinge upon each other and coalesce. The halves of these voids are the shallow dimples visible on the tensile fracture surface. Gradual growth and eventual coalescence of the fine microscopic cracks results in one or more macroscopic cracks that is favored to propagate in the direction of the tensile stress axis. The irreversible plastic deformation that is occurring at the "local" level is responsible for aiding the growth of both the microscopic and macroscopic cracks through the microstructure. The fine microscopic and macroscopic cracks tend to propagate in the direction of the major stress axis, suggesting the important role played by normal stress in promoting tensile deformation. Since a gradual extension of both the microscopic and macroscopic cracks, under quasi-static loading, essentially occurs at the high local stress intensities comparable with the fracture toughness of the material, the presence of a population of fine microscopic and macroscopic voids does exert a detrimental influence on strain-to-failure (ε_f) associated with ductile fracture. A gradual destruction of the microstructure of the titanium material culminates in conditions at the "local" level that are conducive for crack extension to occur at locations of prevailing local high stress intensities. The microscopic cracks tend to propagate in the direction of the tensile stress axis, suggesting the important role of normal stress in enhancing tensile deformation. Since crack extension under quasi- static loading essentially occurs at the high "local" stress intensities comparable with the fracture toughness of the material, the presence of a healthy population of voids, of varying size, has a detrimental influence on strain-to-failure associated with ductile fracture.

5. Conclusions

A study of the tensile deformation and fracture behavior of commercially pure titanium (Grade 2) and Ti-6Al-4V both in the annealed condition provides the following key observations:

1. The as-received commercially pure (Grade 2) in the annealed condition essentially revealed the primary alpha (α) grains intermingled with small pockets of the beta (β) grains. High-magnification observation revealed

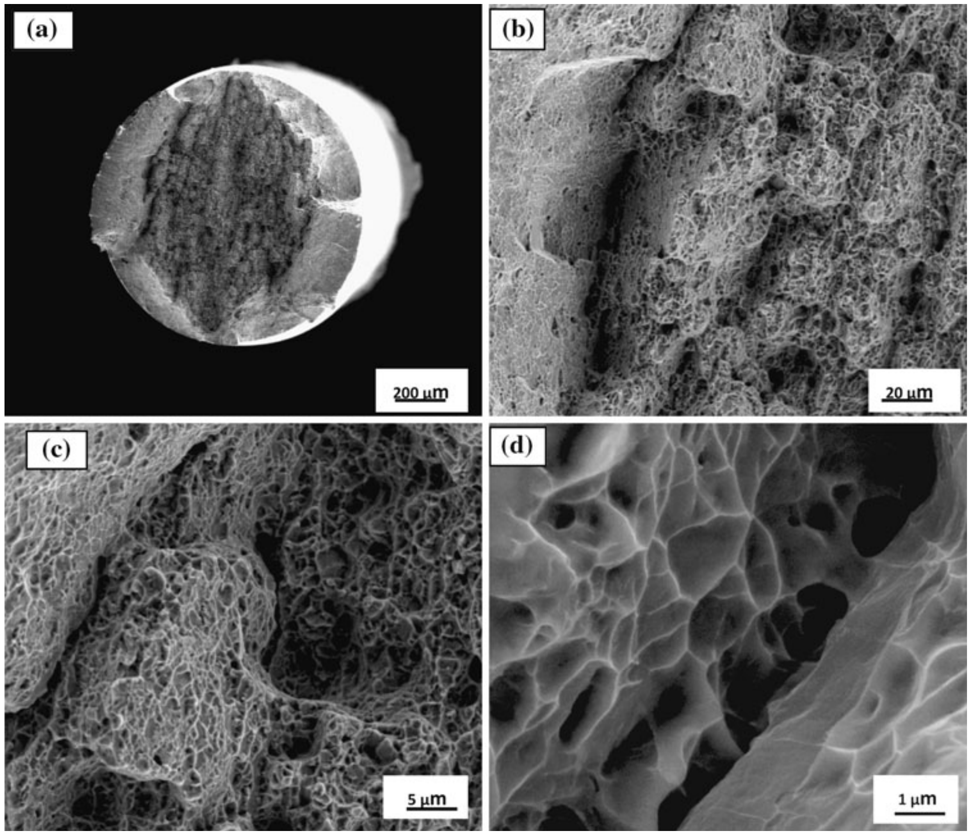

Fig. 11 Scanning electron micrographs of the tensile fracture surface of Ti-6Al-4V specimen (orientation: transverse) deformed in tension, showing (a) overall cup and cone morphology of tensile fracture surface; (b) high magnification of (a) showing microscopic crack, population of voids and dimples in the transgranular region; (c) high magnification of (b) showing the morphology and distribution of microscopic cracks, voids and dimples on the transgranular fracture surface; (d) the overload region showing coalescence of microscopic voids to form a microscopic crack and surrounded by shallow dimples

clearly the alpha (α) phase lamellae located well within the beta (β) grain.

2. The Ti-6Al-4V alloy exhibited a duplex microstructure consisting of the near equiaxed alpha (α) and the transformed beta (β) phases. The primary near equiaxed-shaped alpha (α) grains was well distributed in a lamellar matrix with transformed beta.
3. The Ti-6Al-4V alloy has an elastic modulus of 125 GPa, while the commercially pure (CP: Grade 2) titanium has an average elastic modulus of 115 GPa, both in the longitudinal orientation of the as-provided annealed plates.
4. The yield strength and ultimate tensile strength of CP (Grade 2) is noticeably higher in the longitudinal orientation than in the transverse orientation. In both orientations, the tensile strength is higher than the yield strength indicating the occurrence of noticeable work hardening beyond yield.
5. The yield strength and tensile strength of the Ti-6Al-4V alloy are marginally lower in the longitudinal orientation than in the transverse orientation. The ultimate tensile strength is only marginally higher than the yield strength, indicating the tendency for strain hardening beyond yield to be low.
6. The Ti-6Al-4V alloy in the annealed condition has acceptable ductility quantified in terms of elongation-to-failure and reduction-in-area in both the longitudinal and transverse orientations. The ductility, i.e., elongation-to-failure and reduction-in-area, of the CP (Grade 2) is noticeably higher in both the longitudinal and transverse orientations when compared to the alloy (Ti-6Al-4V) counterpart in conformance with the lower strength of this material when compared to the alloy in both the longitudinal and transverse orientations.
7. Tensile fracture of CP (Grade 2) was at an inclination to the far field tensile stress axis for both longitudinal and transverse orientations. Isolated and randomly distributed microscopic voids and a healthy population of dimples were found covering the transgranular fracture regions. Microscopically, the transgranular region revealed the dimples to be shallow and of varying size coupled with fine microscopic cracks. The overload region revealed a combination of fine microscopic cracks, microscopic voids of varying size and randomly distributed through the surface, and a large population of shallow dimples, features reminiscent of locally brittle and ductile failure mechanisms.
8. Tensile fracture of the Ti-6Al-4V alloy was macroscopically rough and essentially normal to the far field stress axis for the longitudinal orientation and cup-and-cone morphology for the transverse orientation. However, microscopically, the surface was rough and covered with a population of macroscopic and fine microscopic cracks, voids of varying size, a population of shallow dimples of varying size and shape, features reminiscent of locally brittle and ductile failure mechanisms.

Acknowledgments

The authors express and extend most sincere appreciation to the peer reviewer(s) whose comments and suggestions have helped improve the technical significance of this article. Sincere thanks to the Defense Metals Technology Center (DMTC: Canton, OH) for providing financial support for this research study. Thanks and appreciation are also extended to ATI Wah Chang (Oregon) and TICO (Michigan) for providing the material used in this study.

References

1. *ASM Metals Handbook*, Vol 2, 10th edn., Materials Park, OH, 1990, p 586–591
2. M.J. Donachie, Jr., *Titanium—A Technical Guide*, 2nd edn., American Society for Materials International, Materials Park, OH, 2000, p 1–3
3. F.H. Froes, Titanium, *Encyclopedia of Materials Science and Engineering*, P. Bridenbaugh, Ed., Elsevier, Oxford, 2000
4. F.H. Froes, Titanium Metal Alloys, *Handbook of Chemical Industry Economics*, J. Ellis, Ed., Wiley, New York, 2000
5. New Horizons for Aerospace, *R&D Magazine*, January 1996, p 28–30
6. D.R. Askeland, *The Science and Engineering of Materials*, 2nd edn., Thompson Canada Limited, Toronto, Canada, 2007, p 443
7. M. Peters, J. Kumpfert, C. Ward, and C. Leyens, Titanium Alloys for Aerospace Applications, *Adv. Eng. Mater.*, 2003, **5**(66), p 419–427
8. R.R. Boyer, An Overview on the Use of Titanium in the Aerospace Industry, *Mater. Sci. Eng.*, 1996, **A213**, p 103–114
9. J.K. Wessel, Ed., *The Handbook of Advanced Materials*, Oak Ridge, Tennessee, 2004, p 272–319
10. Titanium Alloys Developments, An Overview of Technical Presentations of the 21st Annual ITA Conference, Scottsdale, Arizona, *Adv. Mater. Processes*, 2006
11. V.N. Moiseyev, *Titanium Alloys: Russian Aircraft and Aerospace Application*, Taylor & Francis, 2006
12. D.H. Kohn and P. Ducheyne, Tensile and Fatigue Strength of Hydrogen-Treated Ti-6Al-4V Alloy, *J. Mater. Sci.*, 1991, **26**(2), p 328–334
13. Y.T. Lee, M. Peters, and G. Welsch, Elastic Moduli and Tensile and Physical Properties of Heat-Treated and Quenched Powder Metallurgical Ti-6Al-4V Alloy, *Metall. Trans. A*, 1991, **22**(3), p 709–714
14. D. Makel and D. Eylon, The Effect of Microstructure on Localized Melting at Separation in Ti-6Al-4V Tensile Samples, *Metall. Trans. A*, 1990, **21**(12), p 3127–3136
15. W.R. Kerr, The Effect of Hydrogen as a Temporary Alloying Element on the Microstructure and Tensile Properties of Ti-6Al-4V, *Metall. Trans. A*, 1985, **16**(6), p 1077–1087
16. C.G. Rhodes and N.E. Paton, The Influence of Î±/Î^{2} Interface Phase on Tensile Properties of Ti-6Al-4V, *Metall. Trans. A*, 1979, **10**(11), p 1753–1758
17. A. Arieli and A. Rosen, Superplastic Deformation of Ti-6Al-4V Alloy, *Metall. Trans. A*, 1977, **8**(10), p 1591–1596
18. M. Peter, A. Gysler, and G. Lutjering, Influence of Texture on Fatigue Properties of Ti-6Al-4V, *Metall. Trans.*, 1984, **15A**, p 597–605
19. T.S. Srivatsan and Mithun Kuruvilla, Microstructure, Hardness, Tensile Deformation, Cyclic Fatigue and Fracture Behavior of Ti-Al-V-Fe-O Alloy: Role of Sheet Stock, Final Technical Report, ATI Wah Chang, March 2007
20. C. Bathias, K. El Alami, and T.Y. Wu, Influence of Mean Stress on Ti-6Al-4V Fatigue Crack Growth at Very High Frequency, *Eng. Fract. Mech.*, 1997, **56**(2), p 255–264